Linearization Approach for Symmetric Hysteresis Loop Modelling and Core Loss Prediction

Nenad Petrovic[1], Nebojsa Pjevalica[2],Velibor Pjevalica[3], Nikola Teslic[2]
[1]*School of Electrical Engineering Stari Grad*,
Visokog Stevana 37, 11000 Belgrade, Serbia
[2]*Dept. of Computing and Control Engineering, University of Novi Sad, Faculty of Technical Sciences,*
Trg Dositeja Obradovica 6, 21000 Novi Sad, Serbia
[3]*Technical Provision Section, JP Srbijagas*,
Narodnog fronta 12, 21000 Novi Sad, Serbia
etsstarigrad@sezampro.rs

***Abstract*—First, the paper proposes the method for interpolation of any experimentally obtained symmetric hysteresis loop curve (SHLC) with accuracy and computation efficiency at discrete Fourier transformation (DFT) level. Second, the method has been further developed so that, based on the family of the properly chosen and measured SHLCs, it reliably and accurately predicts an arbitrary inner SHLC. Sinusoidal magnetic flux, along with applied zero crossing sampling system, allows for the introduction of the pure linearization approach. The novelty of this approach is a direct transformation of a cosine polynomial (CP) interpolating of one SHLC over the set of equidistant nodes in the electric angle (EA) domain to the algebraic polynomial (AP) interpolating the same SHLC over the set of nonequidistant Chebyshev nodes in the magnetic flux (MF) domain, with the accuracy remaining unchanged. Based on the results of the interpolation error analyses, the SHLC measurement has been proposed for nonequidistant values of magnetic flux at the loop tip, matching the Chebyshev nodes of the second kind. This is the second novelty which enables a successful prediction of an arbitrary inner SHLC.**

***Index Terms*—Accuracy; error estimation; interpolation; magnetic hysteresis; magnetic losses; transformer cores.**

I. INTRODUCTION

The usage of a properly selected numerical fitting method is a common characteristic of the majority of phenomenological approaches to the magnetic curves analysis and modelling. This applies to the earlier works treating some particular magnetic curves (Widger [1], Rivas, Zamarro, Martin, and Pereira [2]), over the flexible Takacs model [3] numerically parameterized by Meszaros [4] and de la Barriere, Ragusa, Appino and Fiorillo [5] to the most comprehensive and usable models recently developed by Zirka, Moroz, Harrison and Chieza [6], Zirka, Moroz, Harrison, Chieza and Hoidalen [7], [8], and Alonso, Jazebi, and de Leon [9]. It should be noted that the works [6]–[8] are based on the continuous earlier research, referenced in [6], and a careful analysis of certain drawbacks in practical usage of the Jiles-Atherton [10], [11] and Preisach model [12], [13].

Different numerical fitting methods, applied to the different models of magnetic curves, affect error distribution in very specific ways. The authors have generally avoided treating this difficult problem explicitly, and mainly resorted to giving graphical presentation of error distribution in particular cases, and offering a remark regarding the good correlation between the experimental and theoretical results. Therefore, there are no consistent means for the comparative estimation of the accuracy that the proposed methods can offer.

On the other hand, the improved flexibility of the proposed models [6]–[8] usually has as a consequence a very tedious preparation for the numerical computations. As an alternative approach, the interpolation method has been proposed in the symmetric hysteresis loop (SHL) modelling by M. Hoffman and H.-G. Herzog [14]. Unfortunately, this remarkable work does not provide an explicitly derived error estimation of a chosen set of the interpolation nodes for the measured SHLs. Secondly, the very interpolation procedure for an arbitrary SHL prediction was omitted. Given that the base set of the experimentally obtained SHLs is the milestone for the second and higher order reversal curves prediction [6], [7], [14], the accuracy of the interpolated SHLs is an important issue.

The above mentioned works [6]–[9], [14] treat the so called inverse hysteresis models. The first step in each of the proposed models [6], [7], [14] is getting a certain number of SHLs by the measurement at some equidistant values of the magnetic flux or magnetic flux density at the loop tip. This work proposes the SHL measurement at nonequidistant values of magnetic flux at the loop tip matching the Chebyshev nodes of the second kind. Since the treated SHLs are symmetrical, their ascending or descending curves only need to be considered.

The symmetric hysteresis loop curves (SHLC) are measured under sinusoidal magnetic flux (MF) regime and

Manuscript received 12 December, 2016; accepted 22 March, 2017.
This work was partially supported by the Ministry of Education, Science and Technological Development of the Republic of Serbia, under grant number TR32014.

then represented by using the cosine polynomials (CP) in the electrical angle (EA) domain $[-\pi,0]$ with an achieved accuracy at the discrete Fourier transform (DFT) level. Actually, sinusoidal MF allows for the introduction of the pure linearization approach, which in turn allows for the direct transformation of the CP of the form

$$p_n(\theta)=\sum_{k=0}^{n} C_k \cos(k\theta), \tag{1}$$

over the EA domain $\theta\in[-\pi,0]$, to the algebraic one of the form

$$\Pi_n(\phi)=\sum_{k=0}^{n} C_k T_k(\phi/\Phi_m), \tag{2}$$

with the remaining C_k coefficients and accuracy unchanged. The polynomial (2) represents the same SHLC, but now in the MF domain $\phi\in[-\Phi_m,\Phi_m]$. Terms $T_k(\phi/\Phi_m)$ in (2) denote the k degree Chebyshev polynomials of the first kind, whereas ϕ represents the instantaneous MF values, and Φ_m denotes the maximal value of MF at the loop tip. In Section II the linearization approach will be briefly presented and the existence of the discrete sets of samples showing how the method can be applied will be considered. An estimation of the approximation error, as well as the testing of the accuracy of the method by considering distribution of the approximation error for experimentally obtained SHLC, is presented in Section III. In Section IV, this method is further developed for the interpolative prediction of an arbitrary inner SHLC, while the discussion and conclusion is given in Section V and Section VI respectively.

II. THEORY OF LINEARIZATION APPROACH AND EXPERIMENTAL RESULTS

A. Theoretical and Experimental Requirements for the Validity of the Method

Let us assume that the MF in magnetic circuit of an Epstein frame (toroidal specimen) or a single phase transformer at industrial frequency f = 50 Hz or f = 60 Hz is sinusoidal. A generally accepted view in this case is that the extremes of the same sign of the excitation current and the MF occur simultaneously at the moments when the induced electromotive force in the primary and secondary windings achieves zero values (Fitzgerald, Kingsly, Umans [15]).

The previous assumption implies the use of a dual-channel zero crossing system for synchronous sampling. For this purpose, the authors used two Agilent 3458 multimeters in the zero crossing mode with a sampling rate of 10 kHz. One channel was used for the sampling of the excitation current $i_0(t)$ and another for the sampling of the induced electromotive force in the secondary winding $e_0(t)$. The $e_0(t)$ was used as a trigger zero crossing signal, while the power source was the sinusoidal voltage source Fluke 6100 A with f = 50 Hz mains frequency. For this purpose, a single phase transformer 220 V/57.73 V, S_n = 100 VA was used as a measuring object. Along with sample sets of the $i_0(t)$ and $e_0(t)$ obtained by the measurement, the MF samples were obtained by the numerical integration from the $e_0(t)$ samples. The measurements were done for the next series of 13 supply voltages matching the Chebyshev nodes of the second kind. These values are represented in Table I.

TABLE I. RMS SUPPLY VOLTAGE VALUES MATCHING CHEBYSHEV NODES OF THE SECOND KIND.

13.81 V, 41.22 V, 67.98 V, 93.67 V, 117.88 V, 140.23 V, 160.37 V, 177.98 V, 192.78 V, 204.55 V, 213.08 V, 218.26 V, 220.00 V

The above mentioned sampling system enables a set of 200 samples of the excitation current $i_0(t)$ and the electromotive force $e_0(t)$ for an entire period T = 0.02 s, f = 50 Hz. The sampling process is synchronized with regard to the zero values of the $e_0(t)$ signal, which is equal to the synchronization with regard to the extremes of the signals $\phi(t)$ and $i_0(t)$. Therefore, from the set of 200 samples for an entire period T, and by using software processing, a set of 101 samples was selected that belong to the ascending part of the signals $\phi(\theta)$ and $i_0(\theta)$ on the EA domain $\theta\in[-\pi,0]$, $\theta=2\pi t/T$, resulting in $i_0(-\pi)=-I_m$, $i_0(0)=I_m$, $\phi(-\pi)=-\Phi_m$, $\phi(0)=\Phi_m$. In other words, the first sample from this set that corresponds to the negative extreme, for both the MF and the excitation current, was indexed with the index value 0. Then, the last sample from this set that corresponds to the positive extreme for both the MF and the excitation current was indexed with the index value 100. The synchronized sets of 101 samples that belong to the ascending part of the signals $\phi(\theta)$ and $i_0(\theta)$ are graphically shown in Fig. 1.

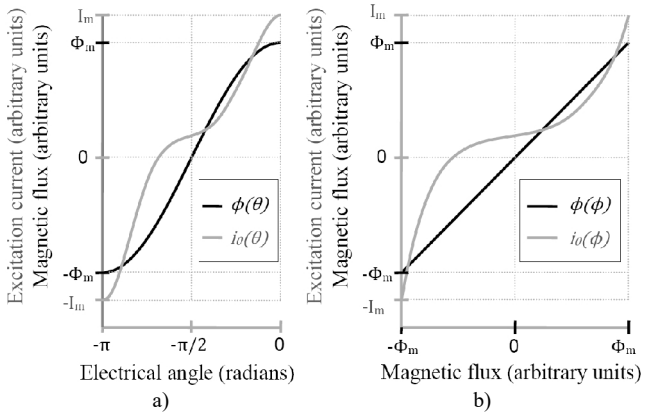

Fig. 1. Waveforms of excitation current (grey line) and magnetic flux (black line) synchronized on the electric angle segment [-π, 0] (a); Excitation current mapping into the ascending hysteresis loop curve (b).

The synchronized set of sinusoidal MF samples actually represents the values of cosine function $\phi(\theta)=\Phi_m\cos\theta$ into the EA domain $\theta\in[-\pi,0]$. By mapping the abscissae domain $\theta\in[-\pi,0]$ by means of the function $\Phi_m\cos\theta$ onto abscissae domain $\phi\in[-\Phi_m,\Phi_m]$, with the ordinates remaining unchanged, the MF samples are perfectly linearly distributed along a straight line of the form $y=x$. As a consequence of the new MF distribution, the excitation current samples will be distributed along the ascending

curve of the hysteresis loop (Petrovic, Pjevalica, Vujicic [16]). This situation is represented fully in Fig. 1. At the same time, the CP (1) of the excitation current will be mapped into an algebraic polynomial (AP) (2) of the hysteresis loop curve ([16], [17]).

Without any loss of generality, and for the purpose of the common mathematical notation usage, the further consideration will be based on the normalized MF values, denoted with $x = \phi / \Phi_m$.

B. Existence of the Subsets of Samples Which Represent the Chebyshev Nodes of the First and the Second Kind

Now the sample index is denoted by k. Then the Chebyhev nodes of the first kind (CHN_I nodes) are determined by the expression [17]:

$$x_{kChI} = cos\theta_{kChI}, \tag{3}$$

$$\theta_{kChI} = -\left(2n_{ChI} - 2k + 1\right)\pi / 2n_{ChI}, \tag{4}$$

where $\left(k = 1,2,\ldots,n_{ChI} < 100\right)$, and the Chebyhev nodes of the second kind (CHN_II nodes) are determined by the expression [17]:

$$x_{kChII} = cos\theta_{kChII}, \tag{5}$$

$$\theta_{kChII} = \left(k/(n_{ChII} - 1) - 1\right)\pi, \tag{6}$$

where $(k = 0,1,\ldots,n_{ChII} - 1)$. By means of the substitution $\Delta\theta = \pi/100$, where $\Delta\theta$ represents the sampling step, expressions (3)–(4) and (5)–(6) get the next form

$$x_{kChI} = cos\left(-\frac{\left(2n_{ChI} - 2k + 1\right) \times 100 \times \Delta\theta}{2n_{ChI}}\right), \tag{7}$$

where $(k = 1,2,\ldots,n_{ChI})$.

$$x_{kChII} = cos\left(\frac{k \times 100}{n_{ChII} - 1} - 100\right)\Delta\theta, \tag{8}$$

where $(k = 0,1,\ldots,n_{ChII} - 1)$. Based on (7), the expression for determining index values of the CHN_I nodes is derived as

$$k_{ChI} = 100 - \frac{\left(2n_{ChI} - 2k + 1\right) \times 100}{2n_{ChI}}, \tag{9}$$

where $(k = 1,2,\ldots,n_{ChI})$. The above expression allows only those values for n_{ChI} that produce the integer values for k_{ChI}. Therefore, n_{ChI} can take only the values from the set {50, 25, 10, 5, 2, 1}. Similarly, from (8) it is obtained

$$k_{ChII} = k \times 100/(n_{ChII} - 1), \tag{10}$$

where $(k = 0,1,\ldots,n_{ChII} - 1)$ and integer values for k_{ChII} will be obtained only if n_{ChII} takes the values from the set {101, 51, 26, 11, 6, 5, 3, 2}.

All possible index values obtained from the expressions (9) and (10) are represented in Table II, except for the values for $n_{ChI} \le 5$ and $n_{ChII} \le 6$. The reason for this is that an expected number of excitation current harmonics is certainly higher then 5. In addition, the index values for $n_{ChII} = 101$ are excluded from the Table II. In the case of $n_{ChII} = 101$, the entire set of samples would be included, making the analysis of the error distribution virtually impossible.

TABLE II. IDENTIFICATION OF THE SAMPLE SUBSETS THAT REPRESENT CHEBYSHEV NODES.

for	Index of the sample that coincides with a node index
$n_{ChI} = 10$	{5, 15, 25, 35, 45, 55, 65, 75, 85, 95}
$n_{ChII} = 11$	{0, 10, 20, 30, 40, 50, 60, 70, 80, 90, 100}
$n_{ChII} = 21$	{0, 5, 10, 15, 20, 25, 30, 35, 40, 45, 50, 55, 60, 65, 70, 75, 80, 85, 90, 95, 100}
$n_{ChI} = 25$	{2, 6, 10, 14, 18, 22, 26, 30, 34, 38, 42, 46, 50, 54, 58, 62, 66, 70, 74, 78, 82, 86, 90, 94, 98}
$n_{ChII} = 26$	{0, 4, 8, 12, 16, 20, 24, 28, 32, 36, 40, 44, 48, 52, 56, 60, 64, 68, 72, 76, 80, 84, 88, 92, 96, 100}
$n_{ChI} = 50$	{1, 3, 5, 7, 9, 11, 13, 15, 17, 19, 21, 23, 25, 27, 29, 31, 33, 35, 37, 39, 41, 43, 45, 47, 49, 51, 53, 55, 57, 59, 61, 63, 65, 67, 69, 71, 73, 75, 77, 79, 81, 83, 85, 87, 89, 91, 93, 95, 97, 99}
$n_{ChII} = 51$	{0, 2, 4, 6, 8, 10, 12, 14, 16, 18, 20, 22, 24, 26, 28, 30, 32, 34, 36, 38, 40, 42, 44, 46, 48, 50, 52, 54, 56, 58, 60, 62, 64, 66, 68, 70, 72, 74, 76, 78, 80, 82, 84, 86, 88, 90, 92, 94, 96, 98, 100}

C. Generating a SHLC Interpolation Polynomial over the Chebyshev Nodes of the First and the Second Kind

The interpolation polynomial over $n_{ChI} = n + 1$ CHN_I nodes from normalized MF domain $x \in [-1,1]$, $x = \phi / \Phi_m$ has the following form [17]

$$P_{n_{ChI}}(x) = \frac{1}{2}c_0 \times T_0(x) + \sum_{k=1}^{n_{ChI}-1} c_k \times T_k(x), \tag{11}$$

where $x \in [-1,1]$. Term $T_k(x)$ in the above expression denotes a *k* degree Chebyshev polynomial of the first kind.

By virtue of the discrete orthogonality [17], [18] of the $T_k(x)$ Chebyshev polynomials over CHN_I nodes, the c_k coefficients are computed by two equivalent expressions:

$$c_k = (2/(n+1)) \sum_{j=1}^{n_{ChI}} i_0(x_j) \times T_k(x_j), \tag{12}$$

$$c_k = (2/(n+1)) \sum_{j=1}^{n_{ChI}} i_0\left(\theta_{jChI}\right) \times \cos\left(k \times \theta_{jChI}\right), \tag{13}$$

where $k = 0,\ldots,n_{ChI} - 1$, $j = 0,\ldots,n_{ChI} - 1$, $x_j = cos(\theta_{jChI})$, and θ_{jChI} is determined by (4).

In accordance with (11), (12) and (13) a cosine interpolation polynomial over n + 1 CHN_I nodes in the EA domain $\theta \in [-\pi, 0]$ has the following form [17]

$$p_{n_{ChI}}(\theta) = \frac{1}{2}c_0 + \sum_{k=1}^{n_{ChI}-1} c_k \times \cos k\theta, \tag{14}$$

where $\theta \in [-\pi, 0]$. An example of generating an

interpolation polynomial by means of (12)–(14) is represented for the set of $n_{ChI} = 10$ Chebyshev nodes of the first kind in tabulated form in Table III and in graphical form in Fig. 2. This polynomial interpolates the ascending SHLC of the most outer hysteresis loop obtained at 220 V supply.

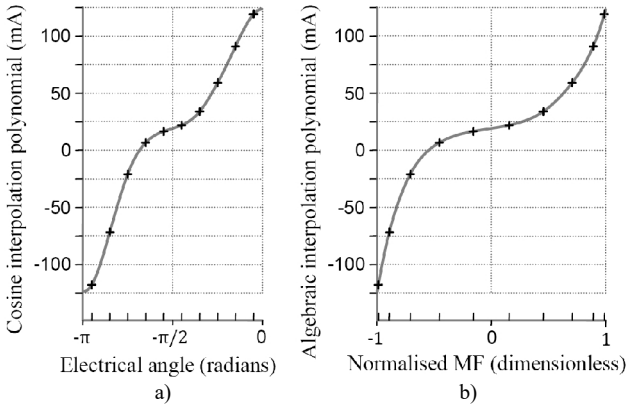

Fig. 2. Graph of the cosine interpolation polynomial over 10 CHN_I nodes in the EA domain θ ∈ [-π, 0] (a); Graph of the algebraic interpolation polynomial over 10 CHN_I nodes in the normalized MF domain x ∈ [-1, 1] (b).

TABLE III. CHEBYSHEV NODES OF THE FIRST KIND AND THE COEFFICIENTS OF THE CORRESPONDING INTERPOLATION POLYNOMIAL.

n_{ChI} node index	sample ϕ (index) [mWb]	sample ϕ(index) normalized	sample i_0(index) [mA]	coefficients for Chebyshev polynomial basis	
5	-1.343223	-0.98768834	-117.73383	c_0	0.0276080973
15	-1.214427	-0.89100652	-71.73744	c_1	0.0897163468
25	-0.966170	-0.70710678	-20.84362	c_2	-0.0095927426
35	-0.621415	-0.45399050	6.71507	c_3	0.0301421501
45	-0.214354	-0.15643446	16.62675	c_4	-0.0048764490
55	0.214354	0.15643446	21.98335	c_5	0.0037755316
65	0.621415	0.45399050	33.87069	c_6	-0.0003212031
75	0.966170	0.70710678	59.07249	c_7	0.0005555446
85	1.214427	0.89100652	90.99124	c_8	0.0004339397
95	1.343223	0.98768834	119.09578	c_9	0.0001550182

Similarly, by virtue of the discrete orthogonality of the $T_k(x)$ Chebyshev polynomials over $n_{ChII} = n+1$ Chebyshev nodes of the second kind [17], the following expressions hold

$$P_{n_{ChII}}(x) = \frac{1}{2}c_0 T_0(x) + \sum_{k=1}^{n-1} c_k T_k(x) + \frac{1}{2}c_n T_n(x), \quad (15)$$

where $x \in [-1,1]$.

$$c_k = \frac{2}{n}\left(\frac{1}{2}i_0(x_0)T_k(x) + \sum_{j=1}^{n-1} i_0(x_j)T_k(x_j) + \frac{1}{2}i_0(x_n)T_k(x_n)\right), \quad (16)$$

$$c_k = \frac{2}{n}\left(\frac{1}{2}i_0(\theta_0) + \sum_{j=1}^{n-1} i_0(\theta_{jChII})\cos(k\theta_{jChII}) + \frac{1}{2}i_0(\theta_{nChII})\cos(k\theta_{nChII})\right), \quad (17)$$

$$p_{n_{ChII}}(\theta) = \frac{1}{2}c_0 + \sum_{k=1}^{n-1} c_k \cos k\theta + \frac{1}{2}c_n \cos n\theta, \quad (18)$$

where $\theta \in [-\pi, 0]$, $k = 0,\ldots,n = n_{ChII} - 1$, $j = 0,\ldots,$ $n = n_{ChII} - 1$, $x_j = cos(\theta_{jChII})$, and θ_{jChII} is determined by the expression (6).

An example of generating an interpolation polynomial by means of (15)–(18) is represented for the set of $n_{chII} = 11$ Chebyshev nodes of the second kind in graphical form in Fig. 3 and in tabulated form in Table IV. The interpolated SHLC is the same as for CHN_I nodes.

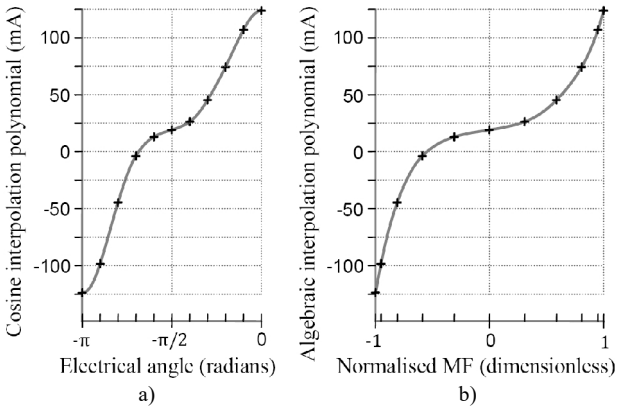

Fig. 3. Graph of the cosine interpolation polynomial over 11 CHN_II nodes in the EA domain θ ∈ [-π, 0] (a); Graph of the algebraic interpolation polynomial over 11 CHN_II nodes in the normalized MF domain x ∈ [-1, 1] (b).

TABLE IV. CHEBYSHEV NODES OF THE SECOND KIND AND THE COEFFICIENTS OF THE CORRESPONDING INTERPOLATION POLYNOMIAL.

n_{ChII} node index	sample ϕ(index) [mWb]	sample ϕ(index) normalized	sample i_0(index) [mA]	coefficients for Chebyshev polynomial basis	
0	-1.359462	-1.000000000	-123.795498	c_0	0.0276971868
10	-1.294644	-0.951056516	-98.412061	c_1	0.0896541475
20	-1.104122	-0.809016994	-44.543009	c_2	-0.0095414213
30	-0.803888	-0.587785252	-3.735111	c_3	0.0300749038
40	-0.423263	-0.309016994	13.030176	c_4	-0.0047526785
50	0.00000	0.000000000	19.154967	c_5	0.0036494057
60	0.423263	0.309016994	26.337257	c_6	-0.0000148624
70	0.803888	0.587785252	45.335193	c_7	0.0004456793
80	1.104122	0.809016994	74.312542	c_8	0.0004815688
90	1.294644	0.951056516	107.005978	c_9	-0.0000286386
100	1.359462	1.000000000	123.795498	c_{10}	-0.0000424001

To generate an AP over the domain of actual values of MF $\phi \in [-\Phi_m, \Phi_m]$, it is necessary to transform an AP $P_k(x)$ from the basis of the Chebyshev polynomials of the first kind $T_k(x)$ into the basis of monomial x^k

$$P_n(x) = \sum_{k=0}^{n} c_k T_k(x) = \sum_{k=0}^{n} C_k x^k. \quad (19)$$

By using the substitution $x = \phi / \Phi_m$ into (19) we obtain an AP over the MF domain $\phi \in [-\Phi_m, \Phi_m]$ of the form

$$\Pi_n(\phi) = \sum_{k=0}^{n} K_k \phi^k. \quad (20)$$

D. Determination of Core Losses by Usage of Interpolation Polynomials: $P_n(x)$ versus $\Pi_n(\phi)$

Figure 4 depicts the closed symmetrical hysteresis loop over the domain $x \in [-1,1]$ that consists of an AP $P_n(x)$ of the form (19) for an ascending SHLC and $-P_n(-x)$, the centrally symmetric to the origin $i_0 - x$ polynomial, for the descending SHLC. The polynomial $P_n(x)$ has the form of (11) for CHN_I nodes, or (15) for CHN_II nodes. The same figure also depicts a closed symmetrical hysteresis loop over the MF domain $\phi \in [-\Phi_m, \Phi_m]$ consisting of polynomials $\Pi_n(\phi)$ (20) and $-\Pi_n(-\phi)$.

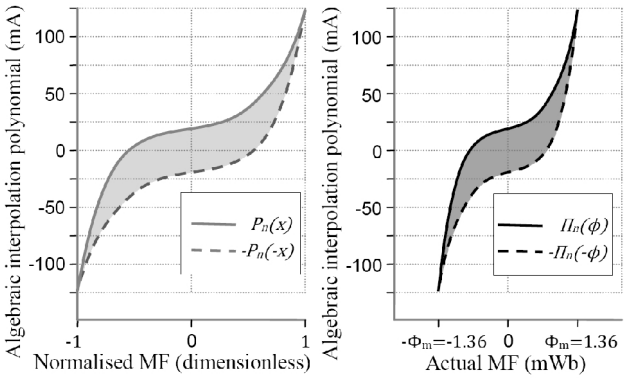

Fig. 4 Hysteresis loop curves approximated by the interpolation polynomials over normalised MF domain (a); Hysteresis loop curves approximated by the interpolation polynomials over actual MF domain (b).

Core losses can be determined by calculating the area of the closed hysteresis loop. Although it seems that this calculation requires the use of the AP form (20)

$$S_{H_\phi} = \int_{-\Phi_m}^{\Phi_m} \left(\Pi_n(\phi) + \Pi_n(-\phi)\right) d\phi, \quad (21)$$

the integration gives as a result

$$S_{H_\phi} = 4\Phi_m \sum_{i=0}^{\lceil n/2 \rceil} (c_{2i}/((2i-1)(2i+1))). \quad (22)$$

In particular, for n+1=10 CHN_I nodes, expression (22) gives

$$S_{H_\phi} = 4\Phi_{\mathrm{m}} \left(\frac{c_0}{2} - \left(\frac{c_2}{1\times 3} + \frac{c_4}{3\times 5} + \frac{c_6}{5\times 7} + \frac{c_8}{7\times 9} \right) \right), \quad (23)$$

and for n + 1 = 11 CHN_II nodes it gives

$$S_{H_\phi} = 4\Phi_{\mathrm{m}} \times \times \left(\frac{c_0}{2} - \left(\frac{c_2}{1\times 3} + \frac{c_4}{3\times 5} + \frac{c_6}{5\times 7} + \frac{c_8}{7\times 9} \right) - \frac{1}{2} \times \frac{c_{10}}{9\times 11} \right). \quad (24)$$

The expressions (22), (23) and (24) point out an important fact regarding numerical calculations, namely, that an area of the closed symmetrical hysteresis loop can be calculated directly on the basis of c_k coefficients and the Φ_m value without the need for generating an AP of the form (20).

III. ANALYSES OF ERROR BEHAVIOUR AND ERROR DISTRIBUTION

A. CHN_I Nodes versus CHN_II Nodes

After transition from the EA domain (time domain) to the algebraic domain (domain of MF), CPs (14) and (18) will be transformed into the APs (11) and (15). This transformation makes possible the distribution function of approximation error

$$e_{n_{Ch}}(x_i) = i_0(x_i) - P_{n_{Ch}-1}(x_i), \quad (25)$$

where $i = 0,...,100$, $x_i \in [-1,1]$, based on the application of Rolle's theorem for the CHN_I nodes, to be expressed in the form

$$e_{n_{ChI}}(x) = i_0(x) - P_{n_{ChI}-1}(x) = = i_0^{(n_{ChI})}(\xi) \frac{T_{n_{ChI}}(x)}{2^{n_{ChI}} \times n_{ChI}!}, \quad (26)$$

where $\min(x, x_0, \ldots, x_{n_{ChI}-1}) < \xi < \max(x, x_0, \ldots, x_{n_{ChI}-1})$, and for CHN_II nodes in the form

$$e_{n_{ChII}}(x) = i_0(x) - p_{n_{ChII}-1}(x), \quad (27)$$

$$e_{n_{ChII}}(x) = i_0^{(n_{ChII})}(\zeta) \frac{(x^2-1) U_{n_{ChII}-2}(x)}{2^{n_{ChII}-1} \times n_{ChII}!}, \quad (28)$$

where $\min(x, x_0, \ldots, x_{n_{ChII}-1}) < \zeta < \max(x, x_0, \ldots, x_{n_{ChII}-1})$.

Terms $T_n(x)$ and $U_n(x)$ in the expressions (26) and (28) represent the Chebyshev polynomials of the first and the second kind of degree n [17].

Since the analytical form of the function $i_0(x)$ is unknown, the expressions (26) and (28) enable the comparison of the quality of approximation for the case when $n_{ChI} = n_{ChII} = n$. In such case, the next expressions hold:

$$\left| \max_{x\in[-1,1]} i_0^{(n)}(x) \right| = M, \quad (29)$$

$$\left| e_{n_{ChI}=n}(x) \right| \le |T_n(x)| \frac{M}{2^n n!} \le \frac{M}{2^n n!}, \quad (30)$$

$$\left| e_{n_{ChII}=n}(x) \right| \le \left| (x^2-1) U_{n-2}(x) \right| \frac{M}{2^{n-1} n!} \le 2 \frac{M}{2^n n!}. \quad (31)$$

The term $i_0^{(n)}(x)$ represents the n-th derivative of the $i_0(x)$ function.

For the practical application, when the interpolation nodes are formed from the set of samples on the basis of (7) and (8) (Table I), will be $n_{ChII} = n_{ChI} + 1$. Then, the impact of

the modulation polynomial $(x^2-1)U_{n_{CHII}-2}(x)$ on the distribution function $e_{n_{ChII}}(x)$ will be favourable toward the impact of the modulation polynomial $T_{n_{CHI}}(x)$ on the distribution function $e_{n_{ChI}}(x)$. This is represented in Fig. 5 for the $n_{ChI}=10$ and $n_{ChII}=11$ case.

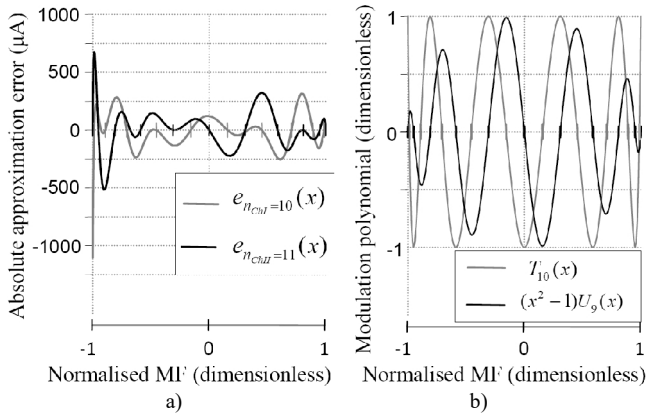

Fig. 5 Graphs of the error distribution functions produced by interpolation polynomials obtained for 10 CHN_I and 11 CHN_II nodes (a); Graphs of the corresponding modulation polynomials for 10 CHN_I and 11 CHN_II nodes (b).

As an illustration of the convergence behaviour, Fig. 6 represents the graphics of the experimentally obtained ascending hysteresis loop curve $i_0(t)$ and its interpolation polynomials for $n_{ChI}=10$, $n_{ChII}=11$, $n_{ChII}=21$, $n_{ChI}=25$ and $n_{ChII}=26$ nodes, together with the corresponding error distribution functions.

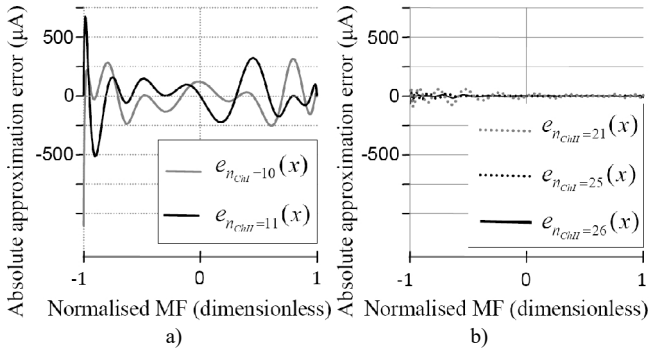

Fig. 6. Graphs of the error distribution functions: (a) for 10 CHN_I – gray and for 11 CHN_II nodes black line; (b) for 21 CHN_II nodes – gray dotted, 25 CHN_I nodes – black dotted and for 26 CHN_II nodes – black solid line.

B. Accuracy Considerations Regarding the Choice of the Kind and the Number of Chebyshev Nodes and Comparison with the DFT Accuracy

Since the analysed SHLC belongs to the most outer hysteresis loop, obtained at 220 V supply, it represents the worst case scenario with regard to the error magnitude. The complete analysis of the all error aspects exceeds the frame of this work and demands an article entirely devoted to this very topic. Instead, the most important facts for interpolation as an approach for the reliable and efficient prediction of an arbitrary inner SHLC will be highlighted here. Two questions arise here about the further interpolation method development: which one of the two kinds of Chebyshev nodes is more suitable for the SHLC application and which number of nodes is needed to obtain a reliable accuracy?

With regard to the first question, there are three good reasons for the choice of the Chebyshev nodes of the second kind. The first is the above analysed impact of the modulation polynomial $(x^2-1)U_{n_{CHII}-2}(x)$ on the error distribution function $e_{n_{ChII}}(x)$, when the interpolation nodes are formed from the set of samples. The second is that the measured loop tips belong to the set of CHN_II nodes. And finally, it has been shown in [19] that for CHN_II nodes usage, the accuracy achieved by using the cosine polynomial is at the level of DFT method proposed in [20].

For an estimation of the accuracy dependence upon the number of CHN_II nodes, the next two aspects will be considered: the accuracy of the closed hysteresis loop area determination and the accuracy of the SHLC instantaneous values determination.

The determination of the closed hysteresis loop area, based on the expressions (21)–(24), gives the results represented in Table V.

Concerning the second aspect, since the relative errors for the all approximated and measured instantaneous values fall below 1 %, whatever number of CHN_II nodes is used, all of the above treated sets of CHN_II nodes could be employed with regard to the achieved accuracy.

TABLE V. RELATIVE ERRORS OF THE CLOSED HYSTERESIS LOOP AREA DETERMINED BY POLYNOMIAL TOWARD THE MEASURED.

Number of nodes	Measured area	Area obtained by polynomial	Relative error [%]
n_{ChII} = 11	9.42364E-05	9.42852E-05	0.051
n_{ChII} = 21	9.42364E-05	9.42528E-05	0.017
n_{ChI} = 25	9.42364E-05	9.42541E-05	0.019
n_{ChII} = 26	9.42364E-05	9.42509E-05	0.015
n_{ChI} = 50	9.42364E-05	9.42513E-05	0.016
n_{ChII} = 51	9.42364E-05	9.42524E-05	0.017

IV. BRIEF EXPLANATION OF THE PROCEDURE FOR AN ARBITRARY INNER SHLC INTERPOLATION

A. Decomposition of a Measured SHLC into its Hysteretic and Anhysteretic Components

As the first step in the interpolation of an arbitrary inner hysteresis loop, it is necessary to decompose each of the measured SHLC to its hysteretic and anhysteretic components

$$i_0(\theta)=i_{anhyst}(\theta)+i_{hyst}(\theta), \tag{32}$$

over EA domain $\theta\in[-\pi,0]$ by using the next two expressions:

$$i_{anhyst}(\theta)=0.5\times\left(i_0(\theta)-i_0\left(-(\theta+\pi)\right)\right), \tag{33}$$

$$i_{hyst}(\theta)=0.5\times\left(i_0(\theta)+i_0\left(-(\theta+\pi)\right)\right), \tag{34}$$

or in normalized MF domain $x\in[-1,1]$ by using:

$$i_{anhyst}(x)=0.5\times\left(i_0(x)-i_0(-x)\right), \tag{35}$$

$$i_{hyst}(x)=0.5\times\left(i_0(x)+i_0(-x)\right). \tag{36}$$

This decomposition has been proposed in [19], [21] and is represented in Fig. 7 for the most outer ascending SHLC measured at 220 V supply. The hysteretic components of all 13 measured ascending SHLCs are represented in Fig. 8.

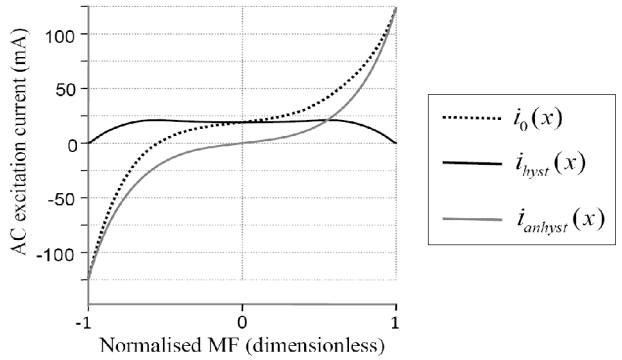

Fig. 7. The most outer ascending SHLC with its hysteretic and anhysteretic components over the domain x ∈ [-1, 1].

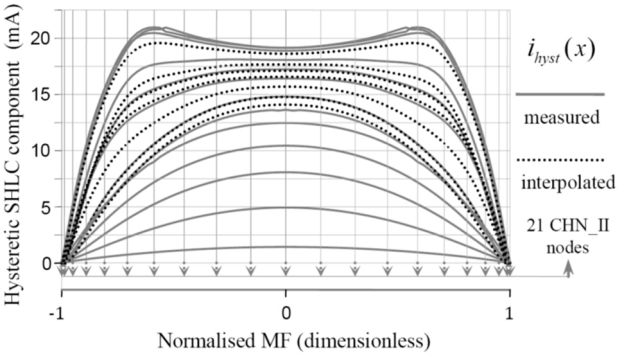

Fig. 8. Measured and interpolated hysteretic SHLC components. The interpolated hysteretic components were calculated for the series of 7 voltage rms values {150 V, 160 V, 170 V, 180 V, 190 V, 200 V, 210 V}.

B. Choice of the Number and Values of Measurement Points

The high interpolation accuracy that CHN_II nodes accomplish for a measured SHLC implies an idea of the measurement of a family of SHLCs at the loop tips matching the CHN_II nodes, instead of the equidistant loop tip values. Since the interpolative prediction of an inner SHLC is actually two-dimensional interpolation, the approximation error should be optimally suppressed. The error analysis (section III A) implies following estimation: the number of CHN_II nodes, that is approximately two times greater than the number of significant harmonics of an excitation current, guarantees the successful suppression of the approximation error (Fig. 6). The sampling frequency of 10 kHz provides two suitable sets of 21 and 26 CHN_II nodes (Table II). This is the main reason why this measurement was performed for 13 rms supply voltage values represented in Table I. Each value produces two peak values that correspond with 26 loop tips of 13 symmetric hysteresis loops. On the other hand, specific number of 13 rms (26 peak-to-peak) CHN_II nodes was limited by the sampling system resolution. This restriction can be observed for hysteretic SHLC components measured in the last three (213.08 V, 218.26 V, 220.00 V) corresponding measurement points (Fig. 8). Finally, 10 kHz sampling frequency choice is in turn determined by the sampling system resolution.

C. Choice of the Number of CHN_II Nodes over the domain x ∈ [-1,1]

The next step is the choice of k_{ChII} CHN_II nodes over the domain $x \in [-1,1]$. These nodes are represented by vertical lines in Fig. 8. For each of these k_{ChII} nodes, the instantaneous value of the function $i_{hyst}(x_k)$ must be determined for an arbitrary chosen value of the supply voltage for the range from 0 V to 220 V. This task is accomplished by using the interpolation polynomials generated at each of x_k nodes, over 13 CHN_II nodes matching the instantaneous values of the measured hysteretic SHLC components. This situation is represented in Fig. 8. Since each of these 13 values is positive, the above mentioned polynomials could be treated as odd, and they are represented by the coefficients with the odd indexes only.

Choice of $k_{ChII} = 21$ instead of $k_{ChII} = 26$ CHN_II nodes in $x \in [-1,1]$ domain decreases computational costs without significant influence on accuracy (Fig. 6). Taking into account that hysteretic component of SHLC is, by definition (36), an even function, the actual number of computations is decreased from 21 to 10. This means that an interpolative prediction of an arbitrary inner hysteretic curve, in this case, resolves 10 vectors consisting of 13 coefficients for each one. These 10 vectors are represented in Table VI.

D. Interpolative Prediction of a Hysteretic Curve for the Given Supply Voltage Value

For an arbitrary supply voltage rms value from the range U ∈ [0 V, 220 V] it is necessary to get its corresponding normalized value x by simple dividing x = U/220 V. Then, this normalized value x is to be submitted to each of the 10 interpolation polynomials represented by its coefficients in Table VI. As a result, 10 interpolated instantaneous values of an inner hysteretic curve $i_{hyst}(x)$ are obtained at 10 of 21 CHN_II nodes. These nodes correspond to the samples with the indexes {5, 10, 15, 20, 25, 30, 35, 40, 45, 50} (Table I and Table VI). The instantaneous values at the first (index 0) and the last (index 100) node take the zero value, by definition of the function $i_{hyst}(x)$. Finally, given that the function $i_{hyst}(x)$ is even, the remaining 9 nodes from the range [0, 1] take the same values as their corresponding nodes from the range [-1, 0]. This correspondence is represented by the following series of the index pairs {(5, 95), (10, 90), (15, 85), (20, 80), (25, 75), (30, 70), (35, 65), (40, 60), (45, 55)}.

Based on knowing 21 CHN_II nodes, the hysteretic curve $i_{hyst}(x)$ can be interpolated by using the polynomial of the form (13), or after the transformation θ = arcos(x) by the polynomial of the form (16). The represented interpolation procedure is applied to 7 values of the supply voltage {150 V, 160 V, 170 V, 180 V, 190 V, 200 V, 210 V} and the interpolated hysteretic curves are represented in Fig. 8. The relative errors obtained by direct measurement of the core losses, and predicted by using the hysteretic curves, are below 0.2 %.

TABLE VI. COEFFICIENTS OF THE POLYNOMIAL INTERPOLATING THE INSTANTANEOUS VALUES OF THE ANHYSTERETIC CURVES AT 10 NODES.

coeff.	node index 5	node index 10	node index 15	node index 20	node index 25
c_1	6.3833E-04	3.4546E-03	7.9931E-03	1.2756E-02	1.6602E-02
c_3	1.9670E-04	1.0753E-03	2.0113E-03	2.5881E-03	2.6902E-03
c_5	2.1206E-04	5.2613E-04	6.4626E-04	7.1113E-04	9.5985E-04
c_7	8.8017E-05	6.5178E-05	-8.7940E-05	-2.6819E-04	-2.6178E-04
c_9	-2.0495E-05	-1.1058E-04	-1.9030E-04	-2.9603E-04	-4.0002E-04
c_{11}	-4.1350E-05	-1.5731E-05	7.9399E-05	1.7102E-04	1.5289E-04
c_{13}	-1.2483E-04	-1.8550E-04	-1.8922E-04	-1.3610E-04	-9.0098E-05
c_{15}	-2.7898E-04	-5.5093E-04	-7.0011E-04	-7.0193E-04	-5.8468E-04
c_{17}	-1.5939E-04	-2.9773E-04	-3.6205E-04	-3.6966E-04	-3.2437E-04
c_{19}	7.6067E-05	1.6202E-04	2.2437E-04	2.3772E-04	2.1392E-04
c_{21}	9.6771E-05	2.0077E-04	2.5467E-04	2.5607E-04	2.1167E-04
c_{23}	9.1052E-06	2.9877E-06	-1.0400E-05	-1.6869E-05	-1.5025E-05
c_{25}	-1.1033E-05	-2.9560E-05	-4.2249E-05	-4.6413E-05	-4.0090E-05
coeff.	node index 30	node index 35	node index 40	node index 45	node index 50
c_1	1.8627E-02	1.9419E-02	1.9914E-02	2.0141E-02	2.0181E-02
c_3	1.8966E-03	5.2897E-04	-5.2013E-04	-1.1451E-03	-1.3525E-03
c_5	1.0653E-03	8.3402E-04	6.4074E-04	5.7865E-04	5.7157E-04
c_7	-9.8832E-05	-5.9372E-05	-9.3847E-05	-1.0767E-04	-1.1173E-04
c_9	-3.2529E-04	-2.3706E-04	-1.6767E-04	-1.2218E-04	-1.0766E-04
c_{11}	1.1990E-04	1.2525E-04	1.2060E-04	1.0806E-04	1.0355E-04
c_{13}	-9.2423E-05	-5.4096E-05	-4.7629E-05	-5.0636E-05	-5.3031E-05
c_{15}	-4.2372E-04	-2.7229E-04	-1.6163E-04	-8.8302E-05	-6.4671E-05
c_{17}	-2.5400E-04	-1.6877E-04	-1.3537E-04	-1.1418E-04	-1.0804E-04
c_{19}	1.6812E-04	1.8134E-04	1.3688E-04	1.0803E-04	9.9642E-05
c_{21}	1.5880E-04	1.2464E-04	5.6321E-05	1.4538E-05	2.9129E-06
c_{23}	-3.3110E-06	3.3478E-05	1.4596E-05	7.8481E-06	7.4156E-06
c_{25}	-3.7999E-05	-3.8834E-06	-1.1123E-05	-1.3649E-05	-1.3739E-05

V. DISCUSSION

Herein all steps of the proposed work will be summarized and the main contributions will be briefly discussed.

The first step is an identification of the sample subsets that represent Chebyshev nodes of the first and the second kind dependent of a given sampling frequency. Expressions (9) and (10) (Section II B) show explicit solution. Generation of the corresponding SHLC approximation polynomial is performed using (11)–(14) and (15)–(18) (Section II C). Described linearization approach gives the first important result – the degree of an approximation polynomial should be equal to the number of significant harmonics of an excitation current or slightly greater, to achieve expected DFT accuracy level.

The successful interpolative prediction of an inner SHLC requires usage of CHN_II nodes, along with decomposition of all measured SHLCs to its hysteretic and anhysteretic components. These issues, along with the choice of optimal subsets of CHN_II nodes, were analysed and resolved through Section III and Section IV.

The interpolative prediction of an arbitrary inner SHLC was tested through prediction of hysteretic SHLC components and its essence is presented in Section IV D. Since the hysteretic component of one SHLC and their interpolation polynomial are both even functions, core losses are predicted directly using (24).

VI. CONCLUSIONS

The linearization approach provides simple and efficient procedure of any magnetic curve approximation by generating an accurate interpolation polynomial. The level of accuracy of these polynomials can be adjusted choosing proper number of Chebyshev nodes, and the level of accuracy can be directly traced and observed. The situation with the fitting functions usage is mainly different, but this important topic exceeds the frame of this work.

The interpolative prediction of an inner SHLC requires that all measured SHLCs have to be decomposed to its hysteretic and anhysteretic component. In that case, the interpolative procedure must be performed over either normalized MF or EA domain. Moreover, generated interpolation polynomial can be transformed into the corresponding one from an actual MF domain without any loss of accuracy.

Finally, sum of both hysteretic (even) and its corresponding anhysteretic (odd) SHLC interpolation polynomial gives the actual SHLC interpolation polynomial.

REFERENCES

[1] G. F. T. Widger, "Representation of magnetisation curves over extensive range by rational fraction approximations", in *Proc. IEEE* vol. 116, 1969, pp. 156–160. Online. [Available]: http://dx.doi.org/10.1049/piee.1969.0032

[2] J. Rivas, L. M. Zamarro, E. Martin, C. Pereira, "Simple approximation for magnetization curves and hysteresis loops", *IEEE Trans. Magn*. vol. 17, no. 4, pp. 1498–1502, 1981. Online. [Available]: http://dx.doi.org/10.1109/TMAG.1981.1061241

[3] J. Takacs, *Mathematics of Hysteretic Phenomena*. N. Y.: Hoboken Wiley/VCH, 2003.

[4] I. Meszaros, "Complex magnetic characterisation of iron-silicon transformer sheets", *Journal of Electrical Engineering*, vol. 57, no. 8/S, pp. 151–154, 2006.

[5] O. de la Barriere, C. Ragusa, C. Appino, F. Fiorillo, "Prediction of energy losses in soft magnetic materials under arbitrary waveforms and DC bias", *IEEE Trans. On Industrial Electronics,* (Accepted for publication) Online. [Available]: http://dx.doi.org/10.1109/TIE.2016.2608886

[6] S. E. Zirka, Y. I. Moroz, R. G. Harrison, N. Chiesa, "Inverse hysteresis models for transient simulation", *IEEE Trans. Power Delivery*, vol. 29, no. 2, pp. 552–559, 2014. Online. [Available]: http://dx.doi.org/10.1109/TPWRD.2013.2274530

[7] S. E. Zirka, Y. I. Moroz, R. G. Harrison, N. Chiesa, H. K. Hoidalen, "Implementation of inverse hysteresis model into EMTP – Part I: static model", *IEEE Trans. Power Delivery*, vol. 30, no. 5, pp. 2224–2232, 2015. Online. [Available]: http://dx.doi.org/10.1109/TPWRD.2015.2416201

[8] S. E. Zirka, Y. I. Moroz, R. G. Harrison, N. Chiesa, H. K. Hoidalen, "Implementation of inverse hysteresis model into EMTP – Part II: dynamic model", *IEEE Trans. Power Delivery*, vol. 30, no. 5, pp. 2233–2241, 2015. Online. [Available]: http://dx.doi.org/10.1109/TPWRD.2015.2416199

[9] C. Alonso, S. Jazebi, F. de Leon, "Experimental parameter determination and laboratory verification of the inverse hysteresis model for single-phase toroidal transformers", *IEEE Trans. Magnetics*, (Accepted for publication). Online. [Available]: http://dx.doi.org/10.1109/TMAG. 2016.2591000

[10] D. C. Jiles, D. L. Atherton, "Theory of ferromagnetic hysteresis", *J. Magnet. Magn. Mater*, vol. 61, pp. 48–60, 1986. Online. [Available]: http://dx.doi.org/10.1063/1.333582

[11] D. C. Jiles, J. B. Thoelke, "Theory of ferromagnetic hysteresis: Determination of model parameters from experimental hysteresis loops", *IEEE Trans. Magn*., vol. 25, no. 5, pp. 3928–3930, 1989. Online. [Available]: http://dx.doi.org/10.1109/20.42480

[12] F. Preisach, "Uber die magnetishe nachwirkung", *Zeit. Physik*, vol. 94, pp. 277–302, 1935. (in German). Online. [Available]: https://doi.org/10.1007/BF01349418

[13] E. Della Torre, "2 The Preisach model". *Magnetic Hysteresis*, pp. 31–51, 1999.

[14] M. Hoffman, H.-G. Herzog, "Modeling magnetic power losses in electrical steel sheets in respect of arbitrary alternating induction waveforms: theoretical considerations and model synthesis", *IEEE Trans. Magn*., vol. 51, no. 2, 2015. Online. [Available]:

http://dx.doi.org/10.1109/TMAG.2014.2353579

[15] A. E. Fitzgerald, C. Kingsly, S. D. Umans, "1.4 AC Excitacion", *Electric Machinery*, pp. 24–28, 2003.

[16] N. Petrovic, V. Pjevalica, V. Vujicic, "The theorem about the transformer excitation current waveform mapping into the dynamic hysteresis loop branch for the sinusoidal magnetic flux case", *Serbian Journal of Electrical Engineering*, vol. 12, no. 1, pp. 33–52, 2015. Online. [Available]: http://dx.doi.org/10.2298/SJEE1501033P

[17] J. C. Masson, D. C. Handscomb, "4.6 Discrete orthogonality of Chebyshev polynomials and 4.7 Discrete Chebyshev transforms and the fast Fourier transform", *Chebyshev polynomials*, 2003.

[18] G. M. Phillips, "2.3 Finite Point Sets", *Interpolation and Approximation by Polynomials*, pp.82–87, 2003.

[19] N. Petrovic, V. Pjevalica, N. Pjevalica, N. Teslic, "Comparative analysis of error distribution for symmetric hysteresis loop curves approximation by means of cosine and trigonometric polynomial", presented at the 2nd Int. Conf. IcETRAN, Silver Lake, Serbia, 2015.

[20] G. Goev, V. Masheva, M. Mikhov, "Fourier analysis of AC hysteresis loops", *IEEE Trans. on Magnetics*, vol. 39, no. 4, pp. 1993–1996, 2003. Online. [Available]: http://dx.doi.org/10.1109/TMAG.2003.814288

[21] N. Pjevalica, N. Petrovic, V. Pjevalica, N. Teslic, "Experimental detection of transformer excitation asymmetry through the analysis of the magnetizing current harmonic content", *Elektronika ir Elektrotechnika*, vol. 22, no. 2, pp. 43–48, 2016. Online. [Available]: http://dx.doi.org/10.5755/j01.eie.22.2.14590